IEEE Access
Multidisciplinary | Rapid Review | Open Access Journal

Received July 16, 2020, accepted August 5, 2020, date of publication August 11, 2020, date of current version August 24, 2020.

Digital Object Identifier 10.1109/ACCESS.2020.3015720

Study on the Control Strategies of Offshore Drilling Crown-Block Heave Compensation System With Compound Cylinders

ZHENDONG LIU[1], YANTING ZHANG[1], XIAOGUANG YU[1], JINGKAI CHEN[1], ZHIKUN WANG[1], DINGYA WANG[2], MINGXING DUAN[3], XINMING MU[2], AND LUMENG HUANG[1]

[1]School of Mechanical and Electronic Engineering, China University of Petroleum (East China), Qingdao 266580, China
[2]CNPC Baoji Oilfield Machinery Company Limited, Baoji 721002, China
[3]China Classification Society, Beijing 100007, China

Corresponding authors: Zhendong Liu (liuzd28@163.com) and Yanting Zhang (ytzhang68@163.com)

This work was supported in part by the National Key Research and Development Plan of China under Grant 2017YFC-0804502 and Grant 2017YFC0804505, in part by the Marine Engineering Research Project of the Ministry of Industry and Information Technology of China (jointed [2014]) under Grant 504, and in part by the special fund project of basic scientific research operating expenses of central universities of China under Grant 18CX02017A.

ABSTRACT To overcome the effect of floating platform heave motion on the drilling operation, a new crown-block heave compensation system with compound cylinders is developed. The new heave compensation system has certain advantages, such as low derrick, short hydraulic pipeline, compact structure, easy operation, etc. The numerical calculation functions of the new heave compensation system are established based on the theories of fluid dynamics and theoretical mechanics. The entire model was built using the Simulink module of MATLAB with a hierarchical structure. As the core component of the compensation system, four control strategies are established to improve the compensation performance, including the PID control, fuzzy control, fuzzy PID control, and Terminal Sliding Mode (TSM) control. Laboratory equipment with a ratio of 1:5 to the new compensation system was designed and developed. The simulation and experimental results show that the new compensation system achieves a good compensation rate of more than 90% under different heave conditions. Among these four strategies, the TSM control strategy generates the highest compensation rate and lowest power fluctuation for the compensation cylinders.

INDEX TERMS Compound cylinder, control strategy, crown-block, drill string heave compensation, offshore drilling platform, terminal sliding mode (TSM), experimental validation.

I. INTRODUCTION

Many countries have been strengthening the exploration and development of deep-sea oil and gas due to their increasing demand. The floating offshore drilling platform produces a rocking motion in six different directions, which are caused by the waves. A drill string heave compensation system is crucial to overcome the heave motion of the platform during the drilling process [1], [2].

Based on the location of installation, the currently used common drill string heave compensation systems include the dead wire rope compensation, winch compensation, traveling block hook compensation, and crown-block compensation [3], [4].

The associate editor coordinating the review of this manuscript and approving it for publication was Ning Sun.

The design of the drill string heave compensation system has been extensively investigated. Jiang proposed a traveling block hook heave compensation system with compound cylinders and analyzed the effects of passive, active, and semi-active compensation methods on the system performance and energy consumption [5]. The traveling block hook heave compensation system is generally used for shallow-water drilling or deep-water exploration ship sampling due to its low compensation load. Huang developed a new semi-active winch heave compensation system with the 2K-H differential planetary gear system to control the outer ring and solar wheel, respectively that compensates for the heave movement and automatically feeds the penetration during the drilling process, and further analyzed the hardware decoupling control of the two movements [6]. Niu developed a semi-active heave compensation system for a 200 T winch

that meets the design requirement to attain up to 92.9% compensation efficiency in the full-scale experiment [7]. However, the steel wire rope in the winch compensation system bears the alternating bending stress and friction force for a long duration. This increases energy consumption and reduces reliability. Liu proposed a streamlined mechanical semi-active heave compensation system with the active compensation part consisting of the driving gear and rack, which drastically improves the performance of the system [8]. The crown-block heave compensation system has been widely utilized due to its advantages such as large bearing capacity, small occupied deck area, high compensation rate, and absence of moving pipeline [9], [10].

Being the core of the compensation system, the control strategy determines the performance of the whole system. Based on the bivariate control model, Huang proposed the Bang-Bang + PID dual-mode control strategy [11]. Li proposed an adaptive double closed-loop controller for the hydraulic valves in the active heave compensation system. An equivalent saturation model was developed using the predictive control method for the inner ring to ensure the angular displacement required for the hydraulic motor tracking process [12]. Shi predicted the motion of the marine platform upon the improvement of the least squares support vector machine by the artificial immune algorithm and achieved better heave compensation performance using the backpropagation neural network PID control strategy [13]. Richter proposed a heave prediction method on the basis of the Levinson recursive least squares algorithm and designed a prediction model for the trajectory planner system, and a 2-DOF controller [14]. Woodacre developed an ocean active heave compensation system with the model predictive controller that decouples transmission motion up to 99.6% [15]. Sun proposed a novel reduced adaptive fuzzy control scheme for a class of stochastic non-strict feedback nonlinear systems with output constraint and unknown control coefficients [16], and adopted fuzzy decoupling control for the lower limb exoskeleton, which is a typical multi-input multi-output uncertain nonlinear system [17]. Based on the high order sliding mode, Yu proposed the ship heave motion compensation and prediction algorithms [18]. However, these control algorithms are not universal. Thus, it is necessary to design a special controller under the specific composition, functional parameters, and motion characteristics of the drill string compensation system.

In this paper, a new crown-block heave compensation system with compound cylinders is proposed. The numerical model of the new heave compensation system is established using the theories of fluid dynamics and theoretical mechanics. Four control strategies, namely PID, fuzzy, fuzzy PID, and Terminal Sliding Mode (TSM), are established. The compensation performances of the four control strategies are discussed. Laboratory equipment is designed and developed to verify comprehensive compensation performance under different working conditions and control strategies.

The remainder of this paper is organized as follows: The new crown-block compensation system with compound cylinders is proposed in Section II. The numerical calculation model of the new compensation system is established in Section III. In Section IV, the PID, fuzzy, fuzzy PID, and TSM control strategies are described along with the optimization of their control parameters. In Section V, the heave compensation comprehensive performances of the four strategies are analyzed by numerical simulation under different sea conditions. Section VI discusses the list of laboratory experiments performed. Finally, the conclusions drawn from the study and their future scopes are included in Section VII.

II. NEW CROWN-BLOCK HEAVE COMPENSATION SYSTEM DESIGN

The compensation system was designed to satisfy the well depth of 10000 m, compensation load of 350 t, heave stroke of 7.62 m, and heave period of 12 s [19]. The overall scheme of the compound cylinder semi-active crown-block compensation system was designed and developed, as shown in Fig. 1.

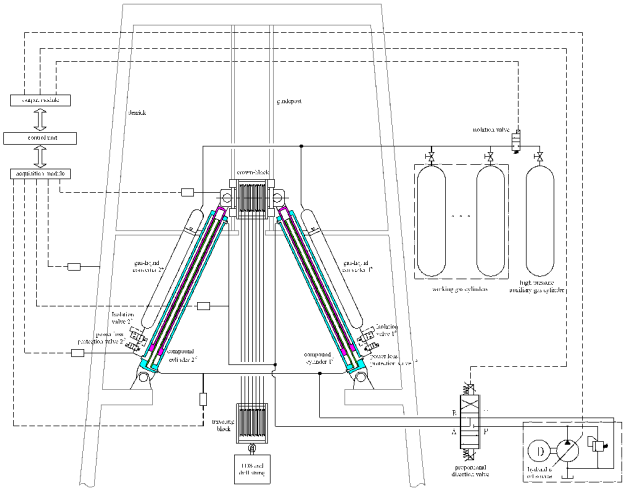

FIGURE 1. The overall scheme diagram of crown-block heave compensation system.

The mechanical system primarily consists of the floating crown-block, swinging device, guidepost, and wire rope. The hydraulic system is composed of the hydraulic oil source, proportional directional valve, compound cylinders, gas-liquid converters, working gas cylinders, high-pressure auxiliary gas cylinder, and isolation valve. The electrical system is made of sensors, signal acquisition module, control unit, and output module.

The compound cylinder is composed of three chambers, namely inner cavity, rod-cavity, and rod-less cavity. The rod-less cavity connects the gas-liquid converter to the working gas cylinders in order to balance the static load of the compensation system. The inner cavity and rod-cavity are connected to ports A and B of the proportional directional valve. Upon obtaining the hydraulic energy output from the

hydraulic oil source, the proportional directional valve causes the compound cylinder piston rod to extend or retract based on certain rules. The semi-active heave compensation function is established by working in combination with the rodless chamber.

The main advantages of the new heave compensation system are as follows:

1) By adopting the compound cylinder technology, the semi-active and passive compensation system functions are established without the incorporation of the independent active cylinder. The simplified structure reduces the height and weight of the derrick. It further reduces the center of gravity of the platform.

2) The working area of the inner cavity is equal to the rod-cavity, and the demand for flow is the same as the piston of the compound cylinder moves. This enables the pump and valve to work properly and achieve a good control effect with ease.

3) When the sea is relatively calm, the system can work in the passive compensation mode. This can be achieved by connecting the rod-cavity to the inner cavity on ceasing the work done by the proportional directional valve since it adopts the Y-type medium function. The hydraulic oil in the two chambers is complementary to each other. The system achieves the passive compensation function using the liquid-air energy storage device.

III. ESTABLISHMENT OF THE NUMERICAL CALCULATION MODEL

The crown-block heave compensation system is mainly composed of the hydraulic oil source, proportional directional valve, compound cylinder, gas-liquid energy storage device, drill string, and hydraulic pipeline. The model of each part is established based on the theories of fluid dynamics and theoretical mechanics as follows.

A. MODEL OF THE HYDRAULIC OIL SOURCE

The hydraulic oil source is composed of the hydraulic pump and overflow valve. The flow-speed equation of the hydraulic pump is:

$$Q_p = n_p V_p \eta_p \tag{1}$$

where Q_p, n_p, V_p, and η_p are the output flow, revolving speed, capacity, and volume efficiency of the hydraulic pump, respectively.

The flow equation of the overflow valve is:

$$Q_{pr} = Q_p - Q_{pv} \tag{2}$$

where Q_{pr} is the flow rate of the overflow valve, and Q_{pv} is the flow rate of the proportional directional valve.

For simplicity, the flow pressure characteristics of the overflow valve are linearized. The valve begins to overflow when system pressure exceeds the set pressure.

B. MODEL OF THE PROPORTIONAL DIRECTIONAL VALVE

The proportional directional valve can be decomposed into two parts, namely, the spool displacement module and the flow output module [20]. Since the parameters of the spool displacement module cannot be acquired accurately, it is difficult to establish an accurate mathematical model. The relationship between the valve displacement x_v, and valve voltage u is simplified as:

$$x_v = k_x u \tag{3}$$

where x_v and u are the displacement and voltage of the proportional directional valve spool, respectively, and k_x is the spool displacement-voltage gain coefficient.

The pressure-flow equations of the four ports in the proportional directional valve are:

$$\begin{cases} Q_{PA} = C_q w x_v \sqrt{\dfrac{2(P_p - P_A)}{\rho}} \\ Q_{BO} = C_q w x_v \sqrt{\dfrac{2\,(P_B - P_t)}{\rho}} \\ Q_{PB} = C_q w x_v \sqrt{\dfrac{2(P_p - P_B)}{\rho}} \\ Q_{AO} = C_q w x_v \sqrt{\dfrac{2\,(P_A - P_t)}{\rho}} \end{cases} \tag{4}$$

where Q_{PA}, Q_{BT}, Q_{PB}, and Q_{AT} are the flow rates of P→A, B→T, P→B, and A→T, respectively. P_p, P_t, P_A, and P_B are the pressures in the direction valve ports P, T, A, and B, respectively. w is the valve orifice area gradient, C_q is the valve port flow coefficient, and ρ is the density of hydraulic oil.

The flow rates of ports A and B in the proportional directional valve is expressed as [21]:

$$\begin{cases} Q_A = C_q w x_v [s_g(x_v) \sqrt{\dfrac{2(P_p - P_A)}{\rho}} \\ \qquad - s_g(-x_v) \sqrt{\dfrac{2\,(P_A - P_t)}{\rho}}] \\ Q_B = C_q w x_v [s_g(x_v) \sqrt{\dfrac{2\,(P_B - P_t)}{\rho}} \\ \qquad - s_g(-x_v) \sqrt{\dfrac{2(P_p - P_B)}{\rho}}] \end{cases} \tag{5}$$

where Q_A and Q_B are the flow rates of the directional valve ports A and B, respectively, and x_v is always negative, which indicates that the valve spool displacement is opposite to the specified positive direction.

The function is defined as:

$$s_g(x_v) = \begin{cases} 1, & x_v \geq 0 \\ 0, & x_v < 0 \end{cases} \tag{6}$$

C. MODEL OF THE COMPOUND CYLINDER

Based on the compressibility of the hydraulic oil and leakage phenomenon in the oil cylinder, the flow continuity equations of the three chambers in the compound cylinder are

as follows [22]:

$$\begin{cases} Q_1 = \dfrac{V_{10} - A_1 x_L}{K_e}\dot{P}_1 - A_1\dot{x}_L + C_t(P_1 - P_2) \\ \qquad +C_t(P_1 - P_3) \\ Q_2 = \dfrac{V_{20} + A_2 x_L}{K_e}\dot{P}_2 + A_2\dot{x}_L + C_t(P_2 - P_1) \\ Q_3 = \dfrac{V_{30} - A_3 x_L}{K_e}\dot{P}_3 - A_3\dot{x}_L + C_t(P_3 - P_1) \end{cases} \tag{7}$$

where Q_1, Q_2, and Q_3 are the flow rates of the rod-less cavity, rod-cavity, and inner cavity of the compound cylinder, respectively. V_{10}, V_{20}, and V_{30} are the volumes of the rod-less cavity, rod-cavity, and inner cavity for the compound cylinder in the equilibrium position, respectively, and V_{20} is equal to V_{30}. A_1, A_2, and A_3 are the working areas of the rod-less cavity, rod-cavity, and inner cavity of the compound cylinder, respectively. P_1, P_2, and P_3 are the working pressure of the rod-less cavity, rod-cavity, and inner cavity of the compound cylinder, respectively. x_L is the displacement of the cylinder piston relative to the compound cylinder block, K_e is the bulk elastic modulus of the hydraulic oil, and C_t is the leakage coefficient of the hydraulic cylinder caused by pressure difference.

The dynamic equilibrium equation of the compound cylinder piston is given by [23], [24]:

$$\begin{cases} F_{bcg} = P_1A_1 + P_3A_3 - P_2A_2 - m_{bc}\ddot{x}_L - c_1\dot{x}_L \\ \qquad -\mathrm{sgn}(\dot{x}_L)(f_{bc} + f_{tc}) \\ f_{bc} = f_c\,(L_{r1} + L_{r2} + L_{r3}) + f_h\,(A_{r1} + A_{r2} + A_{r3}) \end{cases} \tag{8}$$

where F_{bcg} and c_1 are the load and damping coefficient of the compound cylinder, respectively, m_{bc} is the quality of the compound cylinder piston and piston rod, f_{bc} is the frictional force between the compound cylinder piston and piston rod, f_{tc} is the frictional force between the crown-block and its guidepost, f_{c} is the coefficient of friction associated with the seal contact length, L_{r1}, L_{r2}, and L_{r3} are the circumferences of the main piston, main piston rod, and inner cavity plunger piston of the compound cylinder, respectively, f_{h} is the coefficient of friction associated with the seal projected area, and A_{r1}, A_{r2}, and A_{r3} are the seal projected area of the main piston, main piston rod, and inner cavity plunger piston of the compound cylinder, respectively.

D. MODEL OF THE GAS-LIQUID ENERGY STORAGE DEVICE

The gas-liquid energy storage device is primarily composed of working gas cylinders and a gas-liquid converter. The change in the gas state within the working gas cylinders is regarded as an isentropic process. The adiabatic coefficient is set to 1. The compressibility of the hydraulic oil in the gas-liquid converter is ignored. When the piston rod of the compound cylinder moves, the working pressure of the gas in the working gas cylinders is given as follows [25]:

$$P_g = \frac{P_{g0}V_{g0}}{V_{g0} + 2A_4x_{gs}} \tag{9}$$

where P_{g} is the working pressure of the gas cylinders, P_{g0} is equivalent to P_{g} for the system in the equilibrium position, A_4, and x_{gs} are the piston area and piston displacement of the gas-liquid converter, respectively, V_{g} is the sum volume of the gas cylinders and gas chamber of the gas-liquid converter, and V_{g0} is equal to V_{g} for the system in the equilibrium position.

The force equilibrium equation for the piston in the gas-liquid converter is [26]:

$$P_4A_4 = P_gA_4 - m_{gs}\ddot{x}_{gs} - c_1\dot{x}_{gs} - f_{gs} \tag{10}$$

where P_4 is the pressure of the liquid chamber in the gas-liquid converter, m_{gs}, x_{gs}, and f_{gs} are the quality, displacement, and frictional force of the gas-liquid converter piston, respectively.

The flow continuity equation for the liquid cavity in the gas-liquid converter is:

$$Q_4 = \frac{V_{40} - A_4x_{gs}}{K_e}\dot{P}_4 - A_4\dot{x}_{gs} + C_t(P_4 - P_g) \tag{11}$$

where Q_4 is the flow rate in the liquid chamber of the gas-liquid converter, V_{40} is the volume of the liquid cavity for the system under equilibrium.

E. MODEL OF THE DRILL STRING LOAD

Due to the complex dynamic behavior of the drill string, it is simplified into a spring-mass-damping system [27]. The equivalent mass of the drill string is equal to one-third of the total mass of drill string, according to the Rayleigh method in the mechanical vibration theory [28]. The compensation loads such as hook, top drive system, and the equivalent mass of the drill string are simplified to a set of mass m_{eq}. The equilibrium equation of the drill string is [29]:

$$2F_{\mathrm{bcg}}\cos\theta - G = m_{eq}\ddot{x}_h + c_d\dot{x}_h + K_dx_h + f_d + d \tag{12}$$

where:

$$\begin{cases} x_h = x_L\cos\theta - x_s \\ K_d = EA_d\big/L_d \\ c_d = \pi C_N C_I \rho_d D_d \nu_d L_d\big/24 \end{cases} \tag{13}$$

where θ is the angle between the compound cylinder and vertical direction, G is the static load of the compensation system, and m_{eq} is the equivalent dynamic mass of the compensation system including the Top Drive System, hook, traveling block, drill string, etc. x_{h} is the displacement of the hook, x_{s} is the heave displacement of the platform, c_{d} is the mud viscosity, K_{d}, and f_{d} are the equivalent stiffness and frictional force of the drill string, d is the unmodeled resistance, C_{N}, ρ_{d}, and ν_{d} are the friction coefficient, density, and average flow velocity of the drilling fluid, respectively, C_{I} is the additional mass coefficient, L_{d}, A_{d}, D_{d}, and E are the length, cross-sectional area, diameter, and elastic modulus of the drill string.

The viscosity resistance of the drilling fluid increases with the increase in the drilling fluid density, flow rate, and drill pipe length, and cannot be ignored for the drill string length of 10000 m in the hole.

F. MODEL OF THE HYDRAULIC PIPE

The flow continuity equations of the pipeline between the hydraulic pump, proportional directional valve, compensation cylinder, and gas-liquid accumulator are as follows [30]:

$$\begin{cases} Q_{pv} - Q_{PA} - Q_{PB} = \dfrac{V_{pv}}{K_e}\dot{P}_p \\ Q_A - Q_2 = \dfrac{V_{A2}}{K_e}\dot{P}_A \\ Q_B - Q_3 = \dfrac{V_{B3}}{K_e}\dot{P}_B \\ Q_4 - Q_1 = \dfrac{V_{14g}}{K_e}\dot{P}_4 \end{cases} \tag{14}$$

where V_{pv} is the pipeline volume between the hydraulic pump and proportional directional valve, V_{A2} is the pipeline volume between the proportional directional valve port A and the rod-cavity of the compound cylinder, V_{B3} is the pipeline volume between the proportional directional valve port B and the inner cavity of the compound cylinder, and V_{14g} is the pipeline volume between the liquid cavity of the gas-liquid converter and the rod-less cavity of the compound cylinder.

G. MODEL OF THE ENTIRE COMPENSATION SYSTEM

By combining the above six sub-models, the overall model of the crown-block heave compensation system with compound cylinders is established, as shown in Fig. 2. The displacement x_L of the piston rod in the compound cylinder and displacement x_p of the crown block need to be converted by angle θ as the compound cylinder is tilted. This model is built using the hierarchical design in the Simulink software of MATLAB [31].

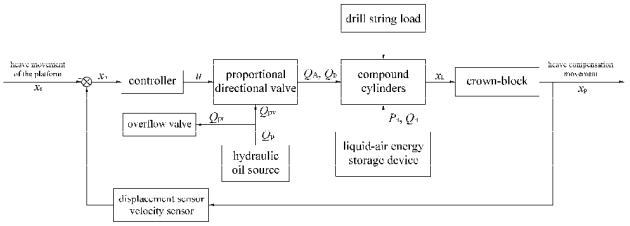

FIGURE 2. The model of the entire compensation system.

The controller is the core component of the compensation system and determines the compensation performance of the entire system. A proper choice of the control strategy can improve the adaptability in sea conditions of the compensation system, and reduce the shutdown time and drilling cost.

The main parameters of the entire simulation model are shown in Table 1.

IV. CONTROL STRATEGY DESIGN

A. TRADITIONAL PID CONTROL STRATEGY

The PID controller has advantages such as the use of simple algorithms, high stability, good reliability, etc.

TABLE 1. The main parameter list of the entire simulation model.

parameter	value	parameter	value
A_1	0.1096 m^2	k_x	0.0008 m/V
A_2	0.00385 m^2	m_{eq}	1.2×10^5 kg
A_3	0.00385 m^2	m_{bc}	3900 kg
c_1	2400	P_{g0}	1.85×10^7 Pa
c_d	6579	P_p	2.1×10^7 Pa
c_q	5.2×10^{-3} m^2/(s·Pa)	V_{10}	0.4 m^3
C_t	1.4×10^{-10} m^3/(s·Pa)	V_{20}	0.014 m^3
f_c	42.5N/m	V_{30}	0.014 m^3
f_h	5.16×10^4N/m^2	V_{40}	0.5 m^3
G	3.5×10^6 N	V_{g0}	21 m^3
K_d	66818.2 N/m	K_e	7×10^8 Pa

The corresponding control difference equation is [32]:

$$u(k) = K_P e(k) + K_I \sum_{j=0}^{i} e(j) + K_D(e(k) - e(k-1)) \tag{15}$$

where $K_I = K_P^* T/T_i$ and $K_d = K_P^* T_d/T$. u represents the output signal of the controller, e is the error signal, T_i and T_d are the integral time constant and differential time constant, respectively. K_P, K_I, and K_D are the proportional, integral, and differential gain coefficients, respectively. T is the sampling period, and i is the sampling sequence number.

The PID parameters were adjusted manually first and then adjusted using the Cohen-Coon method [33]. The step responses of the compensation system are shown in Fig. 3. The fluctuation time is longer upon the adoption of manually adjusted PID parameters. When the PID parameters optimized by Cohen-Coon method are adopted, the system reaches the target value at 8s, and the optimized PID parameters are (10.36, 0.97, 4.33).

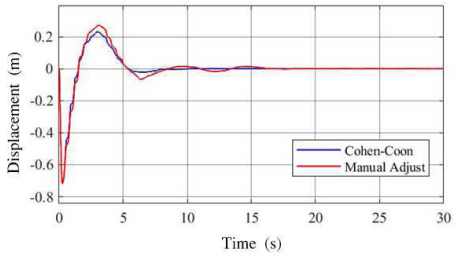

FIGURE 3. The step response of the compensation system under PID control.

B. FUZZY CONTROL STRATEGY

The fuzzy control processes have advantages such as the non-requirement for accurate modeling, strong robustness, strong anti-interference, and simple control principle. Its control structure is shown in Fig 4.

The fuzzy controller selects seven language variables such as {NB, NM, NS, ZE, PS, PM, PB}, discrete domain of the input displacement error E, the rate of change of displacement deviation EC, and the output control quantity U

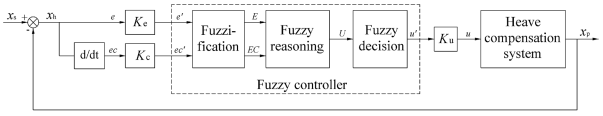

FIGURE 4. Schematic diagram of the fuzzy control.

of values {-6, –5, –4, –3, –2, –1, 0, 1, 2, 3, 4, 5, 6}. Their membership functions are selected to be the triangle, Gaussian, and trapezoid, respectively. The step responses of the compensation system are shown in Fig. 5.

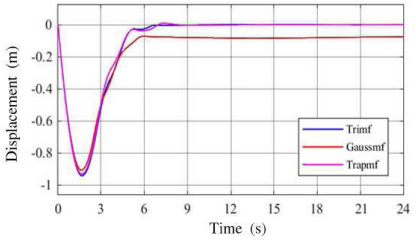

FIGURE 5. The step response of the compensation system under fuzzy control.

It is seen from Fig. 5 that the adoption of trapezoid function results in a steady-state error and small fluctuations for the Gaussian function. The triangle function possesses advantages of fast response, absence of steady-state error, and non-fluctuation. The system reaches the target value at 7 s upon the adoption of the triangle function.

C. FUZZY PID CONTROL STRATEGY

The fuzzy PID control strategy shows good performance in terms of short adjustment time, small overshoot, high steady-state accuracy, and good robustness. The corresponding control structure is shown in Fig. 6. The fuzzy method was used to realize the online automatic adjustment of PID parameters. Thus, it combines the advantages of PID and fuzzy control.

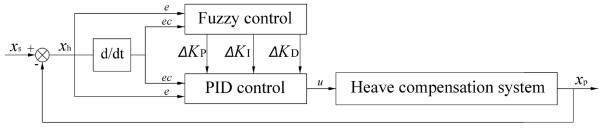

FIGURE 6. Schematic diagram of the fuzzy PID control.

The discrete domains of ΔK_P, ΔK_I, and ΔK_D are {-3, –2, –1, 0, 1, 2, 3}, {-0.6, –0.4, –0.2, 0, 0.2, 0.4, 0.6}, and {-0.3, –0.2, –0.1, 0, 0.1, 0.2, 0.3}, respectively. The triangle function is chosen as their membership function.

The step response effects of the compensation system before and after the fuzzy PID parameter optimization by the Particle Swarm Optimization (PSO) algorithm are shown in Fig. 7 [34].

It is seen from Fig. 7 that the use of the PSO algorithm to optimize fuzzy PID control parameters improves the response

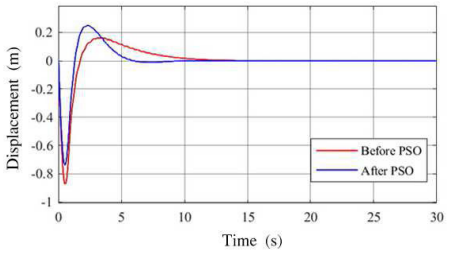

FIGURE 7. The step response of the compensation system under fuzzy PID control.

speed of the compensation system and shortens the time taken to reach the target value from 11 s to 6 s.

D. TSM CONTROL STRATEGY

1) ESTABLISHMENT OF THE STANDARD FEEDBACK FORM EQUATION

The variables are defined as $x = [x_1, x_2, x_3, x_4]^T = [x_p, \dot{x}_p, P_2, P_3]^T$. Thus, the entire system can be expressed in a state-space form as:

$$\begin{cases} \dot{x}_1 = x_2 \\ \dot{x}_2 = \dfrac{2m_{bc}}{2m_{bc}+m_{eq}}[2A_1h_3(x_1) + 2A_3x_4 - 2A_2x_3 - 2c_1x_2 \\ \qquad -G - m_{eq}\ddot{x}_s - c_dg_1(x_2, \dot{x}_s) - K_d(x_1 - x_s) - d] \\ \dot{x}_3 = h_1(x_1)[C_qwk_xug_2(x_3, u) - A_2x_2 - C_t(x_3 - h_3(x_1))] \\ \dot{x}_4 = h_2(x_1)[A_3x_2 + C_qwk_xug_3(x_4, u) - C_t(x_4 - h_3(x_1))] \end{cases} \tag{16}$$

where:

$$\begin{cases} h_1(x_1) = K_e/(V_{20} + A_2x_1) \\ h_2(x_1) = K_e/(V_{30} - A_3x_1) \\ h_3(x_1) = P_{g0}V_{g0}/(V_{g0} + 2A_1x_1) \\ g_1(x_2, \dot{x}_s) = x_2 - \dot{x}_s \\ g_2(x_3, u) = s_g(u)\sqrt{2\left(P_p - x_3\right)/\rho} - s_g(-u)\sqrt{2\left(x_3 - P_t\right)/\rho} \\ g_3(x_4, u) = s_g(u)\sqrt{2\left(x_4 - P_t\right)/\rho} - s_g(-u)\sqrt{2\left(P_p - x_4\right)/\rho} \end{cases} \tag{17}$$

As a practical closed-loop control system, its variables are always constrained. The following assumptions are made.

Assumption 1: The displacement x_L, velocity $\dot{x}_L$, accelerated velocity $\ddot{x}_L$, and differential of acceleration $\dddot{x}_L$ of the compound cylinder are limited.

Assumption 2: The pressure of P_2 and P_3 are limited, with $0 \le P_t \le P_2 \le P_p$, $0 \le P_t \le P_3 \le P_p$.

Equation (16) is converted into a standard feedback form to make use of the back-stepping technique, and a new variable $\bar{x}_3 = x_3 - x_4$ is defined, as A_2 is equal to A_3, the entire system

can be rewritten as:

$$\begin{cases} \dot{x}_1 = x_2 \\ \dot{x}_2 = \dfrac{2m_{bc}}{2m_{bc}+m_{eq}}[2A_1h_3(x_1) - 2A_2\bar{x}_3 - c_1x_2 \\ \qquad -G - m_{eq}\ddot{x}_s - c_df_1 - K_df_2 - d] \\ \dot{\bar{x}}_3 = -f_3x_2 + f_4u - f_5 \\ f_1 = g_1(x_2, \dot{x}_s) \\ f_2 = x_1 - x_s \\ f_3 = h_1(x_1)A_2 + h_2(x_1)A_3 \\ f_4 = C_qwk_x[h_1(x_1)g_2(x_3,u) - h_2(x_1)g_3(x_4,u)] \\ f_5 = h_1(x_1)C_t(x_3 - h_3(x_1)) - h_2(x_1)C_t(x_4 - h_3(x_1)) \end{cases} \tag{18}$$

where $[x_1, x_2, \bar{x}_3] = \left[x_p, \dot{x}_p, x_3 - x_4\right] = \left[x_p, \dot{x}_p, P_2 - P_3\right]$.

As the compensation cylinders require frequent commutation and the gas-liquid energy storage device greatly influences the system performance, a double-loop control structure with displacement tracking as the outer ring and pressure control as the inner ring is designed to decrease the difficulty in adjusting the parameter of the sliding mode controller. The input signal u of the controller is designed based on the reverse step method. The Lyapunov function is constructed to prove that the designed controller satisfies the Lyapunov stability.

2) STRUCTURAL DEVIATION EQUATION

As $e_1 = x_p - x_s = x_1 - x_s$, and $e_2 = \dot{e}_1 = \dot{x}_p - \dot{x}_s$ are defined [35], then:

$$\begin{cases} \dot{e}_1 = e_2 \\ \dot{e}_2 = \ddot{x}_p - \ddot{x}_s = \ddot{x}_1 - \ddot{x}_s = \dot{x}_2 - \ddot{x}_s \\ = \dfrac{2m_{bc}}{2m_{bc}+m_{eq}}[2A_1h_3(x_1) - 2A_2\bar{x}_3 - c_1x_2 - G - \\ \dfrac{m_{eq}\left(2m_{bc}+m_{eq}\right)+2m_{bc}}{2m_{bc}+m_{eq}}\ddot{x}_s - c_df_1 - K_df_2 - d] \end{cases} \tag{19}$$

3) DESIGN OF THE DEVIATION EQUATION VIRTUAL QUANTITY $\bar{\alpha}_3$ BY REVERSE STEP METHOD

The complexity of the nonlinear system was reduced using an inverse step design. The introduction of dummy variables and the construction of the Lyapunov function guarantee the boundness and convergence of the system.

d is the unmodeled uncertainty in the system [36]. It is assumed to be bounded as $|d| < d_{\max}$.

A terminal sliding surface was designed for the compensation system as:

$$S = \dot{e}_1 + \tau e_1^{\alpha_1} = e_2 + \tau e_1^{\alpha_2} \tag{20}$$

where τ and α_1 are positive real numbers. As e_1 decreases or approaches zero, the sliding surface s decreases or tends to zero.

Taking the derivative of both sides of Equation (20):

$$\dot{s} = \dot{e}_2 + \tau\alpha_1 e_1^{\alpha_1 - 1}\dot{e}_1 \tag{21}$$

The Lyapunov function is defined as:

$$V_1 = \frac{1}{2}s^2 \tag{22}$$

Taking the derivative of both sides of Equation (22):

$$\dot{V}_1 = s\dot{s} \tag{23}$$

A virtual control quantity $\bar{\alpha}_3$ was considered as follows:

$$\bar{\alpha}_3 = \frac{1}{2A_2}\left[2A_1h_3(x_1) - c_1x_2 - G - \frac{m_{eq}\left(2m_{bc}+m_{eq}\right)+2m_{bc}}{2m_{bc}+m_{eq}}\ddot{x}_s - c_df_1 - K_df_2 + \frac{2m_{bc}+m_{eq}}{2m_{bc}}\tau\alpha_1 e_1^{\alpha_1 - 1}e_2 + \eta sgn(s)\right] \tag{24}$$

If $\bar{z}_3 = \bar{\alpha}_3 - \bar{x}_3$, then:

$$\begin{aligned} \dot{s} &= \frac{2m_{bc}}{2m_{bc}+m_{eq}}[2A_1h_3(x_1) - 2A_2\bar{x}_3 - c_1x_2 - G \\ &\quad - \frac{m_{eq}\left(2m_{bc}+m_{eq}\right)+2m_{bc}}{2m_{bc}+m_{eq}}\ddot{x}_s - c_df_1 - K_df_2 - d \\ &\quad - 2A_2\bar{\alpha}_3 + 2A_2\bar{\alpha}_3] + \tau\alpha_1 e_1^{\alpha_1 - 1}e_2 \\ &= \frac{2m_{bc}}{2m_{bc}+m_{eq}}[-d - \eta sgn(s) + 2A_2\bar{z}_3] \end{aligned} \tag{25}$$

Substituting Equation (25) into Equation (23):

$$\begin{aligned} \dot{V}_1 = s\dot{s} &= -\frac{2m_{bc}}{2m_{bc}+m_{eq}}d\cdot s - \frac{2m_{bc}}{2m_{bc}+m_{eq}}\eta\cdot|s| \\ &\quad + \frac{4A_2m_{bc}}{2m_{bc}+m_{eq}}\bar{z}_3\cdot s \\ &= -\frac{2m_{bc}}{2m_{bc}+m_{eq}}[\eta + d\cdot sgn(s)]\cdot|s| + \frac{4A_2m_{bc}}{2m_{bc}+m_{eq}}\bar{z}_3\cdot s \\ &\le -\frac{2m_{bc}}{2m_{bc}+m_{eq}}[\eta - |d|]\cdot|s| + \frac{4A_2m_{bc}}{2m_{bc}+m_{eq}}\bar{z}_3\cdot s \end{aligned} \tag{26}$$

4) DESIGN CONTROL LAW U

It was assumed that $\bar{z}_3 = 0$ to ensure the control stability of the system, and thus $\bar{x}_3 = \bar{\alpha}_3$.

Taking the derivative of $\bar{z}_3$:

$$\dot{\bar{z}}_3 = \dot{\bar{\alpha}}_3 - \dot{\bar{x}}_3 = \dot{\bar{\alpha}}_3 + f_3x_2 - f_4u + f_5 \tag{27}$$

The actual output u is designed as:

$$u = \frac{1}{f_4}\left[f_3x_2 + f_5 + \dot{\bar{\alpha}}_3 + c_3\bar{z}_3^{\alpha_2} + \frac{4A_2m_{bc}}{2m_{bc}+m_{eq}}s\right] \tag{28}$$

then:

$$\dot{\bar{z}}_3 = -c_3\bar{z}_3^{\alpha_2} - \frac{4A_2m_{bc}}{2m_{bc}+m_{eq}}s \tag{29}$$

The Lyapunov function was selected as:

$$V = V_1 + \frac{1}{2}\bar{z}_3^2 \tag{30}$$

Taking the derivative of Equation (31):

$$\begin{aligned}\dot{V} &= \dot{V}_1 + \bar{z}_3\dot{\bar{z}}_3 \\ &\le -\frac{2m_{bc}}{2m_{bc}+m_{eq}}\left[\eta - |d|\right]|s| + \frac{4A_2m_{bc}}{2m_{bc}+m_{eq}}\bar{z}_3 s \\ &\quad + \bar{z}_3\left[-c_3\bar{z}_3^{\alpha_2} - \frac{4A_2m_{bc}}{2m_{bc}+m_{eq}}s\right] \\ &\le -\frac{2m_{bc}}{2m_{bc}+m_{eq}}\left[\eta - |d|\right]|s| - c_3\bar{z}_3^{1+\alpha_2} < 0 \qquad (31)\end{aligned}$$

where η is taken to be greater than $d_{\max}$. c_3 is positive, and α_2 is a fraction with odd numbers as the numerator and denominator, and the denominator is bigger than the numerator.

The stability of the designed control system is shown by the Lyapunov stability.

5) CONTROL PARAMETER OPTIMIZATION

The PSO algorithm is used to optimize the main parameters of the TSM controller, such as α_1, α_2, τ, η, etc. The step response effects of the compensation system before and after optimization are shown in Fig. 8. The optimized TSM parameters are $\alpha_1 = 5/7$, $\alpha_2 = 1$, $\tau = 3$, and $\eta = 7.46 \times 10^5$.

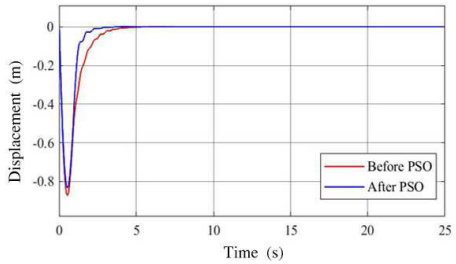

FIGURE 8. The step response of the compensation system under TSM control.

It is seen from Fig. 8 that the TSM control has advantages of fast response, absence of overshoot, and zero fluctuation. Also, the time to reach the target value is shortened from 5 s to 4 s using the PSO algorithm to optimize the TSM control parameters.

V. SIMULATION RESULT AND ANALYSIS

A. ANALYSIS OF VARIOUS PARAMETERS UNDER THE GIVEN HEAVE CONDITION

The semi-active compensation effects of the four control strategies under the sinusoidal heave condition of amplitude 2.5 m and a cycle of 12 s are shown in Fig. 9, Fig. 10, Fig. 11 and Fig. 12.

It is seen from Fig. 9 that the maximum steady-state displacement of the hook is 0.143 m, 0.112 m, 0.096 m, and 0.072 m, respectively, and the compensation ratio is 94.28%, 95.52%, 96.16%, and 97.12%, respectively for PID, fuzzy, fuzzy PID, and TSM control strategies. The TSM strategy has the highest displacement compensation effect among the four control strategies.

It is seen from Fig. 10, Fig. 11, and Fig. 12 that the maximum working pressure of the active chamber is 20.8 MPa

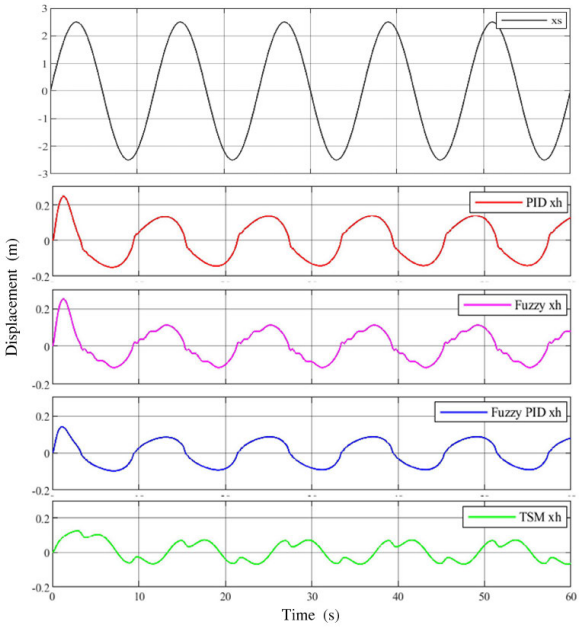

FIGURE 9. The comparison of the compensation effect under the sinusoidal heave condition (2.5 m, 12 s).

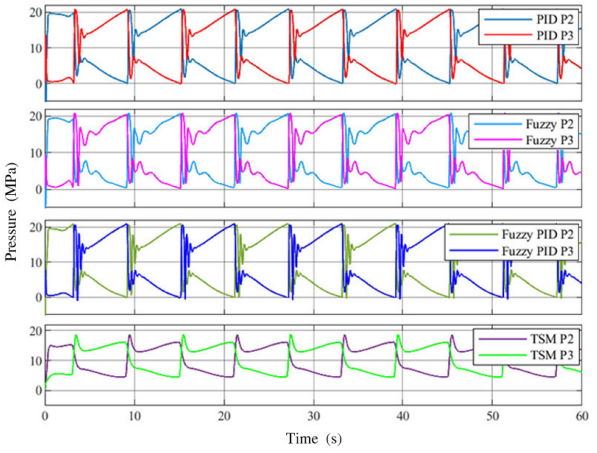

FIGURE 10. The comparison of active chamber pressure under the sinusoidal heave condition (2.5 m, 12 s).

for PID, fuzzy, and fuzzy PID control strategies. However, the maximum working pressure of the active chamber for the TSM control strategy is only 18.7 MPa. The maximum flow of the active chamber is 0.0095 m^3/s, and the peak power of the semi-active compensation system is 189 kW in the four control strategies. However, the average power of the semi-active compensation system is 120.9 kW, 123.1 kW, 121.9 kW, and 116.5 kW for PID, fuzzy, fuzzy PID, and TSM control strategies, respectively.

The fluctuation amplitudes for the pressure and flow curve of the active chamber are the largest under the fuzzy PID control strategy and the smallest under the TSM strategy. Compared to the PID and fuzzy controls, the fuzzy PID control strategy achieves a better compensation effect through quick adjustment.

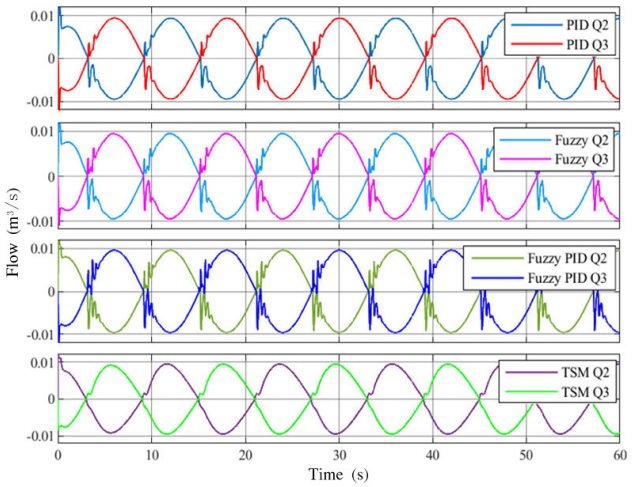

FIGURE 11. The comparison of active chamber flow under the sinusoidal heave condition (2.5 m, 12 s).

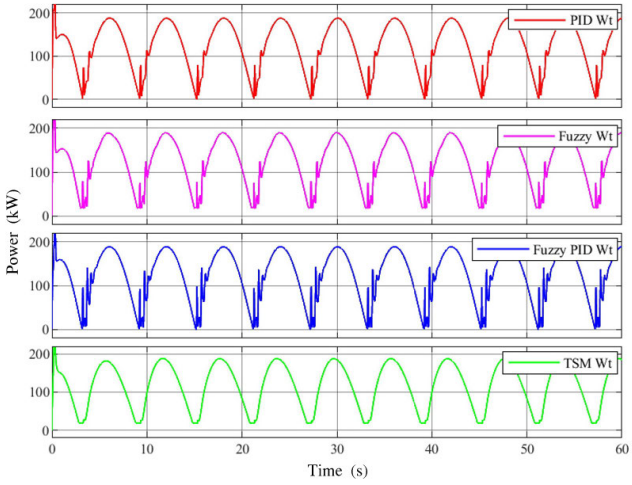

FIGURE 12. The comparison of semi-active compensation power under the sinusoidal heave condition (2.5 m, 12 s).

During the adoption of the TSM control strategy, the power curve of the semi-active compensation system has no obvious fluctuation, and the average power is small compared to the other three control strategies.

B. ANALYSIS OF THE COMPENSATION EFFECT UNDER DIFFERENT HEAVE CONDITIONS

The compensation effects of the four control strategies under the random heave condition of amplitude 3.81 m and a cycle of 12 s are shown in Fig. 13. It is seen from the simulation results that the maximum displacement of the hook is 0.237 m, 0.192 m, 0.179 m, and 0.159 m, respectively, for PID, fuzzy, fuzzy PID, and TSM control strategies.

The comparison of the compensation ratio of the four control strategies under different heave conditions are shown in Table 2 and Fig. 14, under 2.5 m sinusoidal heave, 2.5 m random heave, 3.81 m sinusoidal heave, and 3.81 m random heave conditions.

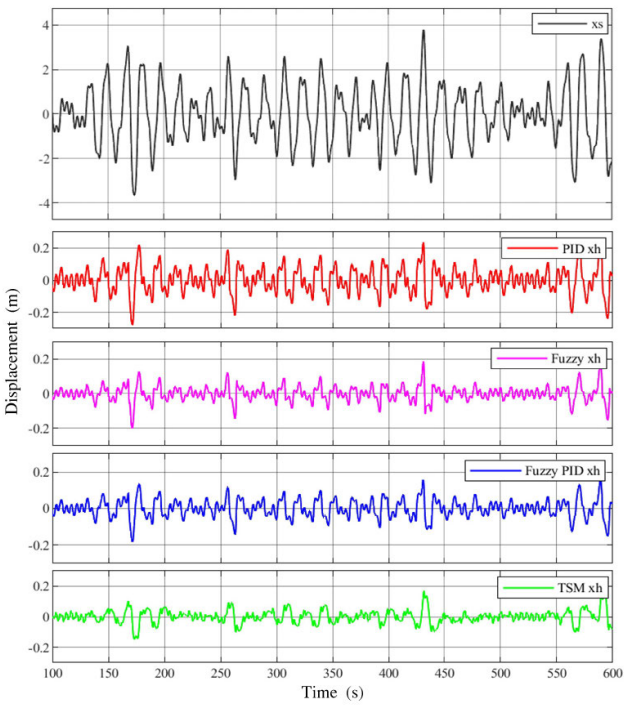

FIGURE 13. The comparison of the compensation effect on random heave condition (3.81 m, 12 s).

TABLE 2. The comparison table of compensation effect under different heave conditions.

Heave condition	PID	Fuzzy	Fuzzy PID	TSM
2.5 m sinusoidal	94.28%	95.52%	96.16%	97.12%
2.5 m random	94.08%	95.32%	96.04%	96.8%
3.81 m sinusoidal	94.04%	95.19%	95.51%	96.03%
3.81 m random	93.92%	94.96%	95.3%	95.83%
Average	94.08%	95.25%	95.75%	96.45%

It is seen from Fig. 14 that the compensation rates of the PID and fuzzy controls are low among the four control strategies. However, the difference in the compensation rates under the four working conditions is small, which proves that the stabilities of PID and fuzzy controls are good. The compensation rate of fuzzy PID control is higher than that of the fuzzy control, with just a difference of 0.86% in the compensation rate under the four working conditions. This proves that the response speed and compensation accuracy of the fuzzy PID control is high. Although the compensation rates of the TSM control under the four operating conditions differ by 1.29%, which is larger than that of the other three control strategies, the compensation rate is always the highest. This proves that the TSM control has good response speed, reliability, and robustness.

The system power comparison of the four control strategies under different heave conditions is shown in Table 3 and Fig. 15 with 2.5 m sinusoidal heave and 3.81 m sinusoidal heave.

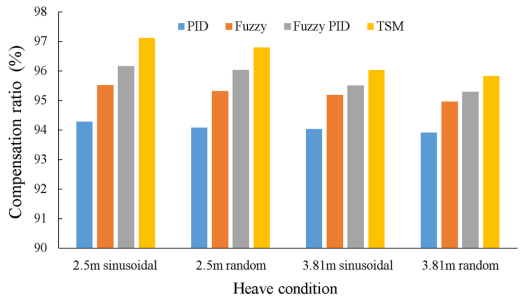

FIGURE 14. The comparison of the compensation effect under different heave conditions.

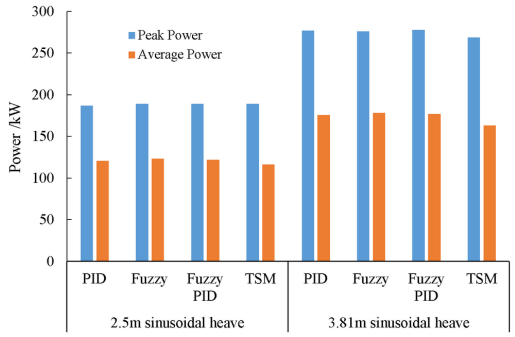

FIGURE 15. The comparison of the system power under different heave conditions.

TABLE 3. The comparison table of the system power under different heave conditions.

Heave condition		PID	Fuzzy	Fuzzy PID	TSM
2.5m sinusoidal	Peak Power/kW	187	189	189	189
	Average Power/kW	120.9	123.1	121.9	116.5
3.81m sinusoidal	Peak Power/kW	277	276	278	269
	Average Power/kW	175.6	178.4	177	163.1

It is seen from Fig. 15 that the peak power of the four control strategies are basically equal, but the average power of the TSM control is the lowest. This is due to the less fluctuating pressure and flow curve, and low invalid work during the compensation process under the TSM control strategy.

VI. SYSTEM EXPERIMENTAL VERIFICATION

The laboratory equipment with a ratio of 1:5 to the new crown-block heave compensation system, with a design load of 2.8 t, and a compensating stroke of 1.2 m is shown in Fig. 16.

The laboratory equipment does not simulate the heave motion of the platform directly but achieves the effect of heave motion of the platform by simulating a change in the force. As the piston rod of the heave simulation cylinder extends or retracts, the simulated load of the drill string is changed through the wire rope. After the signal is detected by the system, the piston rod of the compensation compound cylinder is driven to retract or extend to achieve the effect of the compensating heave motion.

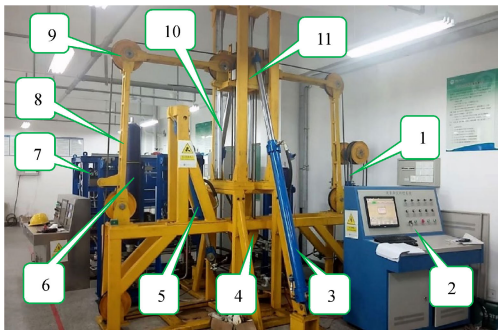

FIGURE 16. The laboratory equipment for the crown-block heave compensation system. 1 Heave Simulation Cylinder, 2 Control Cabinet, 3 Heave Compensation Compound Cylinder, 4 Traveling-block, 5 Drill String Load Simulation Cylinder, 6 Hydraulic Accumulator, 7 Hydraulic Power Unit, 8 Swing Arm, 9 Pulley, 10 Guidepost, 11 Crown-block.

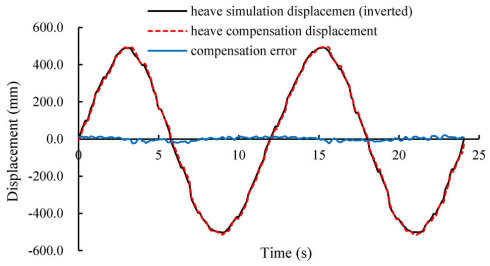

FIGURE 17. The compensation effect of the laboratory equipment under sinusoidal heave condition (500 mm, 12 s) using the fuzzy PID control strategy.

TABLE 4. The compensation rate comparison table of the laboratory equipment under different control strategies.

Compensation rate	PID	Fuzzy	Fuzzy PID	TSM
Minimum	90.8%	92.8%	93.9%	94.8%
Maximum	94.1%	95.0%	95.5%	96.6%
Average	92.6%	93.8%	94.7%	95.8%

The compensation effect of the control system is verified using a matrix experiment performed under the simulated heave amplitude of 200–500 mm, heave period of 8–15 s, and four control strategies. The experimental compensation effect under the fuzzy PID control with the amplitude of 500 mm and heave period of 12 s is shown in Fig. 17.

It is seen from Fig. 17 that the compensation compound cylinder closely follows the motion of the heave simulation cylinder, with the maximum error not exceeding 26.3 mm and a compensation rate of 94.7%.

The compensation effects of the four control strategies are obtained from various experimental data, as shown in Table 4.

It is seen from the above test results that the new semi-active crown-block heave compensation system achieves a good compensation effect under different heave conditions and different control strategies, among which TSM control is the best.

VII. CONCLUSION

In this study, a new semi-active crown-block heave compensation system with compound cylinders has been proposed. This could be achieved through the optimization of the cavity area of the compound cylinder, simultaneous establishment of the semi-active control and passive compensation system function, ceased operation of the separate cylinder system, simplification of the system structure, and effective reduction of the height and weight of the derrick. Especially, the reduction in the center of gravity height of the platform is most conducive.

The dynamic numerical calculation model of the new crown-block heave compensation system is established. Four control strategies, namely, PID, fuzzy, fuzzy PID, and TSM, are designed for the compensation system. The comprehensive performance of the four strategies is analyzed by numerical simulation under different sea conditions. The results show that the compensation rate is more than 94%, with the TSM control strategy generating the highest compensation rate of 97%. Among the four control strategies, the TSM control offers advantages such as fast response, high reliability, good robustness, high compensation rate, absence of overshoot, low pressure and flow fluctuation, low energy consumption, etc.

According to the principle of similitude, laboratory equipment with a ratio of 1:5 to the new crown-block heave compensation system is designed and developed. The comprehensive compensation performance of the experiment system under different working conditions and control strategies has been tested. The results show that the compensation rate is more than 90%. The feasibility and effectiveness of the proposed scheme and control strategies of the new semi-active crown-block heave compensation system have been verified.

In future studies, new control strategies will be introduced to increase the compensation rate of the heave compensation system. Also, the energy-saving technologies for hydraulic systems such as secondary regulation and load sensitivity will be studied.

REFERENCES

[1] P. Gu, A. A. Walid, Y. Iskandarani, and H. R. Karimi, "Modeling, simulation and design optimization of a hoisting rig active heave compensation system," *Int. J. Mach. Learn. Cybern.*, vol. 4, no. 2, pp. 85–98, Apr. 2013.

[2] T. Liu, G. Iturrino, D. Goldberg, E. Meissner, K. Swain, C. Furman, P. Fitzgerald, N. Frisbee, J. Chlimoun, J. Van Hyfte, and R. Beyer, "Performance evaluation of active wireline heave compensation systems in marine well logging environments," *Geo-Mar. Lett.*, vol. 33, no. 1, pp. 83–93, Feb. 2013.

[3] J. K. Woodacre, R. J. Bauer, and R. A. Irani, "A review of vertical motion heave compensation systems," *Ocean Eng.*, vol. 104, pp. 140–154, Aug. 2015.

[4] T. Xiao, J. Huang, and Y. Ge, "Simulation and control of heave compensation winch for ultra-depth floating drilling," in *Proc. IEEE Int. Conf. Cybern. Intell. Syst. (CIS) IEEE Conf. Robot., Autom. Mechatronics (RAM)*, Nov. 2017, pp. 609–613.

[5] H. Jiang, Y. Liu, Y. Zhang, Z. Liu, and L. Bai, "Design float active drillstring heave compensation system of the float drilling Platform," *Acta Petrolei Sinica*, vol. 33, pp. 483–484, Mar. 2012.

[6] L. Huang, Y. Zhang, L. Zhang, and M. Liu, "Semi-active drilling drawworks heave compensation system," *Petroleum Explor. Develop.*, vol. 40, no. 5, pp. 665–670, Oct. 2013.

[7] W. Niu, W. Gu, Y. Yan, and X. Cheng, "Design and full-scale experimental results of a semi-active heave compensation system for a 200 t winch," *IEEE Access*, vol. 7, pp. 60626–60633, 2019.

[8] Q. Liu, Y. Tang, C. Huang, and C. Xie, "Study on a mechanical semi-active heave compensation system of drill string for use on floating drilling platform," *PLoS ONE*, vol. 10, no. 7, Jul. 2015, Art. no. e0133026.

[9] X. Huang, J. Wang, Y. Xu, Y. Zhu, T. Tang, and M. Lv, "Research on heave compensation control of floating crane based on permanent magnet synchronous motor," in *Proc. Int. Conf. Control, Autom. Inf. Sci. (ICCAIS)*, Oct. 2018, pp. 331–336.

[10] Z. Yan-ting, Z. Wen-kai, L. Zhen-dong, Li-An, J. Hao, and Q. Ying-feng, "Virtual experiment and research for heave compensation system," in *Proc. Int. Conf. Fluid Power Mechatronics*, Aug. 2011, pp. 277–282.

[11] J. Huang, T. Xiao, and L. Chen, "Study of control mode and control strategy for direct drive volume control actuating unit of heave compensation winch," in *Proc. IEEE Int. Conf. Cybern. Intell. Syst. (CIS) IEEE Conf. Robot., Automat. Mechatronics (RAM)M*, Ningbo, China, Nov. 2017, pp. 576–580.

[12] Z. Li, X. Ma, Y. Li, Q. Meng, and J. Li, "ADRC-ESMPC active heave compensation control strategy for offshore cranes," *Ships Offshore Struct.*, vol. 12, pp. 1–9, Dec. 2019.

[13] M. Shi, S. Guo, L. Jiang, and Z. Huang, "Active-passive combined control system in crane type for heave compensation," *IEEE Access*, vol. 7, pp. 159960–159970, 2019.

[14] M. Richter, S. Schaut, D. Walser, K. Schneider, and O. Sawodny, "Experimental validation of an active heave compensation system: Estimation, prediction and control," *Control Eng. Pract.*, vol. 66, pp. 1–12, Sep. 2017.

[15] J. K. Woodacre, R. J. Bauer, and R. Irani, "Hydraulic valve-based active-heave compensation using a model-predictive controller with non-linear valve compensations," *Ocean Eng.*, vol. 152, pp. 47–56, Mar. 2018.

[16] W. Sun, S.-F. Su, Y. Wu, and J. Xia, "A novel adaptive fuzzy control for output constrained stochastic non-strict feedback nonlinear systems," *IEEE Trans. Fuzzy Syst.*, early access, Jan. 29, 2020, doi: 10.1109/TFUZZ.2020.2969909.

[17] W. Sun, J.-W. Lin, S.-F. Su, N. Wang, and M. J. Er, "Reduced adaptive fuzzy decoupling control for lower limb exoskeleton," *IEEE Trans. Cybern.*, early access, Feb. 26, 2020, doi: 10.1109/TCYB.2020.2972582.

[18] H. Yu, J. Wei, J. Fang, G. Sun, and H. Zhang, "Predictive robust control based on higher-order sliding mode for passive heave compensator with hydraulic transformer," in *Proc. BATH/ASME Symp. Fluid Power Motion Control*, Bath,U.K., Oct. 2018. Art. no. V001T01A017.

[19] L. Huang, Y. Zhang, M. Liu, and M. Qi, "Design for a drawworks heave compensation system of floating drilling platform," *Acta Petrolei Sinica*, vol. 34, pp. 569–573, Mar. 2013.

[20] H. Xu, Z. M. Guang, and Y. Y. Qi, "Hydrodynamic characterization and optimization of contra-push check valve by numerical simulation," *Ann. Nucl. Energy*, vol. 38, no. 6, pp. 1427–1437, Jun. 2011.

[21] S. Li, J. Wei, K. Guo, and W. Zhu, "Nonlinear robust prediction control of hybrid active–passive heave compensator with extended disturbance observer," *IEEE Trans. Ind. Electron.*, vol. 64, no. 8, pp. 6684–6694, Aug. 2017.

[22] I. Yung, C. Vázquez, and L. B. Freidovich, "Robust position control design for a cylinder in mobile hydraulics applications," *Control Eng. Pract.*, vol. 69, pp. 36–49, Dec. 2017.

[23] G.-C. Lee, J.-S. Kim, J.-H. Kweon, and J.-H. Choi, "Optimal design of composite stiffened cylinder subject to external hydrostatic pressure," *Adv. Sci. Lett.*, vol. 15, no. 1, pp. 297–300, Aug. 2012.

[24] E. Brian, "Research for dynamic friction modeling in linear motion hydraulic piston applications," M.S. thesis, Dept. Mech. Eng., Texas Univ., Austin, TX, USA, 2005.

[25] G. W. Mair, B. Becker, S. John, and E. Duffner, "Composite storage systems for compressed hydrogen–systematic improvement of regulations for more attractive storage units," *Int. J. Hydrogen Energy*, vol. 45, no. 25, pp. 13672–13679, May 2020.

[26] H. Shi, C. Zhao, Z. Liu, and F. Cao, "Study on hydraulic system efficiency of heaving-buoy wave energy converter," *J. Ocean Univ. China*, vol. 17, no. 5, pp. 1044–1052, Oct. 2018.

[27] Q. Xue, H. Leung, L. Huang, R. Zhang, B. Liu, J. Wang, and L. Li, "Modeling of torsional oscillation of drillstring dynamics," *Nonlinear Dyn.*, vol. 96, no. 1, pp. 267–283, Apr. 2019.

[28] Q.-T. Tran, K.-L. Nguyen, L. Manin, M.-A. Andrianoely, R. Dufour, M. Mahjoub, and S. Menand, "Nonlinear dynamics of directional drilling with fluid and borehole interactions," *J. Sound Vib.*, vol. 462, Dec. 2019, Art. no. 114924, doi: 10.1016/j.jsv.2019.114924.

[29] X.-R. Wang, B.-J. Sun, P.-Y. Luo, Z.-Y. Wang, N. Wang, K. Ke, and H. Zhang, "Transient temperature and pressure calculation model of a wellbore for dual gradient drilling," *J. Hydrodyn.*, vol. 30, no. 4, pp. 701–714, Aug. 2018.
[30] H. Dedić-Jandrek and S. Nižetić, "Small scale archimedes hydro power plant test station: Design and experimental investigation," *J. Cleaner Prod.*, vol. 231, pp. 756–771, Sep. 2019.
[31] J. Yan, X. Guo, G. Tan, and T. Yang, "Research on hydraulic retarder control system based on co-simulation," *J. Syst. Simul.*, vol. 23, pp. 1244–1250, Jun. 2011.
[32] A. Khalid, K. Zeb, and A. Haider, "Conventional PID, adaptive PID, and sliding mode controllers design for aircraft pitch control," in *Proc. Int. Conf. Eng. Emerg. Technol. (ICEET)*, Feb. 2019, pp. 1–6, doi: 10.1109/CEET1.2019.8711871.
[33] A. Azman, M. Rahiman, N. Mohammad, M. Marzaki, M. Taib, and M. Ali, "Modeling and comparative study of PID Ziegler Nichols (ZN) and Cohen-Coon (CC) tuning method for multi-tube aluminum sulphate water filter (MTAS)," in *Proc. IEEE 2nd Int. Conf. Autom. Control Intell. Syst. (I2CACIS)*, Kota Kinabalu, Malaysia, Oct. 2017, pp. 25–30.
[34] W. Wu and L. Gao, "Parameter optimization of a stability-training platform's 4-PSS/PS parallel mechanism based on training ability evaluation index and PSO algorithm," *Chin. J. Mech. Eng.*, vol. 31, no. 1, p. 50, Dec. 2018.
[35] S.-Y. Chen and S.-S. Gong, "Speed tracking control of pneumatic motor servo systems using observation-based adaptive dynamic sliding-mode control," *Mech. Syst. Signal Process.*, vol. 94, pp. 111–128, Sep. 2017.
[36] W. Sun, Y. Wu, and Z. Sun, "Command filter-based finite-time adaptive fuzzy control for uncertain nonlinear systems with prescribed performance," *IEEE Trans. Fuzzy Syst.*, early access, Jan. 17, 2020, doi: 10.1109/TFUZZ.2020.2967295.

ZHENDONG LIU received the B.E. degree in mechanical design and manufacturing and automation and the M.E. degree in mechatronic engineering from the China University of Petroleum (East China), China, in 2005 and 2007, respectively, where he is currently pursuing the Ph.D. degree of mechanical engineering. His current research interests include mechatronics and offshore oil equipment.

YANTING ZHANG received the Ph.D. degree in fluid power transmission and control from Zhejiang University, Hangzhou, China, in 2006. He is currently a Professor and the Doctoral Advisor of mechanical engineering with the China University of Petroleum (East China), Qingdao, China. His research interests include offshore oil equipment and fluid transmission and control.

XIAOGUANG YU received the B.E. degree in mechanical design and manufacturing and automation from Xiangtan University, Xiangtan, China, in 2018. He is currently pursuing the master's degree of mechatronic engineering with the China University of Petroleum (East China), Qingdao, China. His current research interests include design and control strategy optimization of offshore oil equipment.

JINGKAI CHEN received the B.E. degree in mechanical design and manufacturing and automation and the M.E. degree in petroleum mechatronic engineering from the China University of Petroleum (East China), Qingdao, China, in 2010 and 2012, respectively, and the Ph.D. degree in mechanical engineering from Rice University, Houston, TX, USA, in 2017. He is currently a Postdoctoral Fellow with the China University of Petroleum (East China). His current research interests include peridynamics, stochastic vibration, and applications.

ZHIKUN WANG received the M.E. degree in safety science and engineering from the China University of Petroleum (East China), Qingdao, China, in 2015, where he is currently pursuing the Ph.D. degree of mechanical engineering. His current research interests include fluid transmission and control engineering.

DINGYA WANG received the M.E. degree in mechanical design and theory from the Southwest China Petroleum Institute, Chengdu, China, in 2003. He is currently the Dean of the Baoji Oilfield Machinery Company Ltd. Research Institute. His current research interests include oil and gas drilling equipment technology on land and sea.

MINGXING DUAN received the M.E. degree in oil-gas well engineering from the China University of Petroleum, Beijing, China, in 2009. He is currently a Senior Engineer with the China Classification Society, Beijing. His current research interest includes offshore oil equipment inspection technology.

XINMING MU received the M.E. degree in mechatronic engineering from Xi'an Technological University, Xi'an, China, in 2006. She is currently a Senior Engineer with the Baoji Oilfield Machinery Company Ltd. Research Institute, Chengdu, China. Her current research interests include the offshore oil and gas drilling equipment.

LUMENG HUANG received the B.E. degree in mechanical design and manufacturing and automation and the Ph.D. degree in mechatronic engineering from the China University of Petroleum (East China), Qingdao, China, in 2009 and 2015, respectively. He is currently a Lecturer and a Master's Supervisor with the China University of Petroleum (East China). His current research interest includes electromechanical control.